Nano-ghosts

Novel biomimetic nano-vesicles for the delivery of antisense oligonucleotides

Oieni, Jacopo; Lolli, Andrea; D'Atri, Domenico; Kops, Nicole; Yayon, Avner; van Osch, Gerjo J.V.M.; Machluf, Marcelle

DOI
10.1016/j.jconrel.2021.03.018

Publication date
2021

Document Version
Final published version

Published in
Journal of Controlled Release

Citation (APA)
Oieni, J., Lolli, A., D'Atri, D., Kops, N., Yayon, A., van Osch, G. J. V. M., & Machluf, M. (2021). Nano-ghosts: Novel biomimetic nano-vesicles for the delivery of antisense oligonucleotides. *Journal of Controlled Release*, *333*, 28-40. https://doi.org/10.1016/j.jconrel.2021.03.018

Journal of Controlled Release 333 (2021) 28–40

Contents lists available at ScienceDirect

Journal of Controlled Release

journal homepage: www.elsevier.com/locate/jconrel

Nano-ghosts: Novel biomimetic nano-vesicles for the delivery of antisense oligonucleotides

Jacopo Oieni [a], Andrea Lolli [b,c], Domenico D'Atri [a], Nicole Kops [b], Avner Yayon [d], Gerjo J.V. M. van Osch [b,e,f], Marcelle Machluf [a,*]

[a] Department of Biotechnology and Food Engineering, Technion - Israel Institute of Technology, Haifa 32000, Israel
[b] Department of Orthopaedics, Erasmus MC, University Medical Center, Rotterdam 3015GD, the Netherlands
[c] Department of Oral and Maxillofacial Surgery, Erasmus MC, University Medical Center, Rotterdam 3015GD, the Netherlands
[d] Procore Ltd., Weizmann Science Park, 7 Golda Meir St., Ness Ziona 7414002, Israel
[e] Department of Otorhinolaryngology, Head and Neck Surgery, Erasmus MC, University Medical Center, Rotterdam, 3015GD, the Netherlands
[f] Department of Biomechanical Engineering, Faculty of Mechanical, Maritime, and Materials Engineering, Delft University of Technology, 2628, the Netherlands

ARTICLE INFO

Keywords:
Nano-ghosts
Nanovesicles
Drug delivery
Antisense oligonucleotides
microRNA
Tissue engineering

ABSTRACT

Antisense oligonucleotides (ASOs) carry an enormous therapeutic potential in different research areas, however, the lack of appropriate carriers for their delivery to the target tissues is hampering their clinical translation. The present study investigates the application of novel biomimetic nano-vesicles, Nano-Ghosts (NGs), for the delivery of ASOs to human mesenchymal stem cells (MSCs), using a microRNA inhibitor (antimiR) against miR-221 as proof-of-concept. The integration of this approach with a hyaluronic acid-fibrin (HA-FB) hydrogel scaffold is also studied, thus expanding the potential of NGs applications in regenerative medicine.

The study shows robust antimiR encapsulation in the NGs using electroporation and the NGs ability to be internalized in MSCs and to deliver their cargo while avoiding *endo*-lysosomal degradation. This leads to rapid and strong knock-down of miR-221 in hMSCs *in vitro*, both in 2D and 3D hydrogel culture conditions (>90% and > 80% silencing efficiency, respectively). Finally, *in vivo* studies performed with an osteochondral defect model demonstrate the NGs ability to effectively deliver antimiR to endogenous cells. Altogether, these results prove that the NGs can operate as stand-alone system or as integrated platform in combination with scaffolds for the delivery of ASOs for a wide range of applications in drug delivery and regenerative medicine.

1. Introduction

In the last 20 years, a vast class of synthetic antisense oligonucleotides (ASOs) has rapidly emerged as a new approach for several therapeutic strategies. [1] ASOs can be considered a sub-group of the larger oligonucleotides-based drugs class. ASOs sub-group comprises different molecules with two main mechanisms of action: RNase H-mediated degradation and steric blockage. The former is activated by gapmeRs molecules and the latter by microRNAs (miRNAs) inhibitors (antimiRs) and splice switching oligonucleotides (SSOs). [1–3] Especially antimiRs have gained increasing attention in several fields since far more than 1000 miRNAs have been identified, and studies have proved their pivotal involvement in the physio-pathological regulation of nearly every tissue. [4,5] Therapies based on the regulation of miRNAs have been demonstrated as a promising regenerative medicine approach for cardiac, muscular, bone and other tissues. [6–9] To exert their functions on preventing miRNAs to bind their messenger RNAs (mRNAs) target, antimiRs must reach the target tissue, penetrate the cell membrane and reach the cytoplasm where they operate. [10] Unfortunately, the potential of ASOs is counteracted by high susceptibility to nucleases and fast clearance that halter the progression in the clinic of numerous treatments. [11]

The most common approach for stabilizing ASOs is the introduction of chemical modifications of the ASOs structure to enhance their target molecule and stability and to reduce nuclease activity [2]. These modifications, however, do not provide the ASOs with targeting abilities needed to deliver them to the target tissue. Hence, the need for efficient carriers for ASOs delivery is the current focus of extensive research, especially using nano-carriers. [12–14] The major drawback in loading the ASOs in nano-vesicles (NVs) is their strong anionic nature, and

* Corresponding author at: Faculty of Biotechnology and Food Engineering, room 428; Technion – Israel Institute of Technology (IIT), Haifa 3200003, Israel.
E-mail address: machlufm@tx.technion.ac.il (M. Machluf).

https://doi.org/10.1016/j.jconrel.2021.03.018
Received 5 December 2020; Received in revised form 8 March 2021; Accepted 12 March 2021
Available online 16 March 2021

therefore the preferable nano systems studied so far are based on complexation with cationic lipids. [15] Other strategies that have been developed are PEGylation of cationic NVs, the introduction of neutral lipids, the use of a variety of synthetic nanocarriers, and the encapsulation in anionic NVs and extra-cellular vesicles. [12] However, many of these strategies lack tissue-specific targeting, do not allow a scalable production process, and show evidence of immunogenicity. [12,16] To overcome these hurdles, several strategies have been developed to design suitable and improved systems to deliver ASOs, such as conjugation to different moieties, non-viral nano-carriers and biomimetic NVs. [12,17]

In recent years, our group has focused on the design and the development of a novel class of natural biomimetic NVs derived from mesenchymal stem cells (MSCs), termed Nano-Ghosts. [18,19] The NGs are derived from the MSCs' cytoplasmic membrane, preserving its composition and properties in terms of the different biomarkers, and are produced *via* a scalable process that maintains such configuration. [19,20] These characteristics empower the NGs with the targeting abilities and immune evasiveness of MSCs, as previously shown in our works targeting cancer sites and without triggering immune responses; moreover, their nano size allows them to deliver different therapeutics including proteins and plasmid DNA for cancer gene therapy. [18,21–23] In the present study, we aimed to validate the NGs as a new carrier for ASOs. As proof of concept, we selected an antimiR molecule targeted to miR-221 (antimiR) that we previously used to stimulate cartilage repair by implanted or endogenous MSCs. [24,25] We evaluated their loading and capability to target MSCs and deliver antimiR to induce miR-221 silencing. We also addressed the possible use of a hydrogel/NGs delivery system to deliver ASOs, *in vivo*, in an osteochondral defect model to establish the possibility to apply our strategy to reach endogenous cells *in situ* thus broadening its application also to the regenerative medicine field.

2. Materials and methods

2.1. Cell cultures

Human bone marrow-derived MSCs for NGs production were purchased from Lonza™ (Basel, Switzerland) and cultured in α-MEM supplemented with 10% fetal bovine serum (FBS), 1% penicillin-streptomycin (P/S) solution, 0.8% Fungizone™, and basic fibroblast growth factor (5 ng mL^{-1}) (bFGF, Peprotech, Rehovot, Israel). Human smooth muscle cells (SMCs, #PCS-420-012, ATCC) were cultured in DMEM high-glucose (Sigma-Aldrich™, Saint Louis, MO) supplemented with 10% FBS and 1% P/S solution. Cultures were maintained at 37 °C in a humidified incubator with 5% CO_2 and relative humidity of 95%. Unless stated otherwise, all cell culture media and supplements were purchased from Biological Industries (BI, Bet-Ha'Emek, Israel). Human bone marrow-derived MSCs for *in vitro* studies were obtained from femoral biopsies of donors (age 50–78 years) undergoing total hip replacement, after signing informed consent and with approval of the local ethical committees (Erasmus MC METC-2015-644; Albert Schweizer Hospital 2011.07). Cells from bone marrow aspirates were seeded at a density of approximately 50,000 nucleated cells cm^{-2} in α-MEM medium supplemented with 10% FBS, bFGF (1 ng mL^{-1}) (AbD Serotec, Oxford, UK), ascorbic acid-2-phosphate (25 mg mL^{-1}) (Sigma-Aldrich™, Saint Louis, MO), Fungizone™ (1.5 mg mL^{-1}) and gentamicin (50 mg mL^{-1}). Non-adherent cells were washed off after 24 h, and adherent cells were further expanded. At subconfluence, MSCs were trypsinized and re-plated at a density of 2300 cells cm^{-2}. The medium was refreshed twice a week and expanded cells at passage 2 to 4 were used for the experiments.

2.2. NGs production and characterization

NGs were produced as previously published and as briefly described below. [18,21] When indicated, for *in vitro* and *in vivo* tracking fluorescent-labelled NGs were obtained by incubating MSCs with fluorescent lipophilic tracers 1,1'-Dioctadecyl-3,3,3′,3'-Tetramethylindodicarbocyanine Perchlorate (DiD) or 3,3'-Dioctadecyloxacarbocyanine Perchlorate (DiO) (1.25 μg mL^{-1}) (Life Technologies™, Carlsbad, CA) for 3 h prior to NGs preparation. Then, cells were treated with tris-magnesium hypotonic buffer, followed by a mild homogenization process (DIAX100 homogenizer, Generator 8F tip, Heidolph Instruments) and a series of centrifugation steps to remove cytosolic content, obtaining cytoplasm-free cells (ghosts). The ghosts' membranes were then fractionated by sonication (VibraCell VCX750, Sonics&Materials) to their final size (~ 200 nm), creating the NGs. The NGs were collected by ultracentrifugation using Sorvall™ WX+ Ultracentrifuge Series (ThermoFisher Scientific, Waltham, MA) at 45000 rpm, 45 min, 4 °C. The final product was resuspended in the desired buffer of use and PEGylated by incubation with Methoxypolyethylene glycol succinate N-hydroxysuccinimide 5000 (Sigma-Aldrich™, Saint Louis, MO) for 2 h at room temperature (RT) in a ratio of 10:1 PEG-to-proteins weight-to-weight (w w^{-1}), calculated by Bradford assay (Bio-Rad, Hercules, CA). PEGylation was stopped by the addition of L-lysine, and excess unreacted PEG and L-lysine were removed using Bio-spin® P-30 Tris Chromatography Columns (Bio-Rad, Hercules, CA) according to the manufacturer's instructions. Phospholipids concentration in the NGs samples was determined using LabAssay phospholipid kit (Wako, Osaka, Japan) according to the manufacturer's instructions. NGs' size and size distribution were analyzed using NanoSight NS300 (Malvern Instruments, Malvern-Worcestershire, UK), while ζ-potential was analyzed with Zetasizer Nano-Series (Malvern Instruments, Malvern-Worcestershire, UK). In all studies reported NGs amount is presented as μg of phospholipids and NGs concentration as μg of phospholipids per mL (w w^{-1}).

2.3. AntimiR-221 loading in NGs

The loading of the NGs with antimiRs was performed *via* electroporation. AntimiR was the ASO used for *in vitro* experiments and is a DNA-based single strain oligonucleotide (20-mer) carrying lock nucleic acid (LNA)-modified bases intersperse in the sequence. Power-antimiR presents LNA-modified bases and phosphorothioate (P—S) backbone modification, but with a shorter sequence (15-mer) and a different arrangement of the LNA-modified bases, that makes it more stable in biological fluids. 6-FAM 5′-labelled miRCURY LNA miRNA inhibitor miR-221-3p (antimiR; Qiagen, Hilden, Germany), 6-FAM 5′-labelled miRCURY LNA miRNA "Power" inhibitor miR-221-3p (Power-antimiR; Qiagen, Hilden, Germany), or miRCURY LNA mismatch scramble control (antimiR-Scr; Qiagen, Hilden, Germany) were added to the NGs in hypo-osmolar electroporation buffer (Eppendorf, Hamburg, Germany) at 0.0625:1 antimiR-to-NGs (w w^{-1}) ratio (replicates >3). The NGs were then electroporated in a 2-mm gap cuvette (Cell projects, Harrietsham, UK) at 2500 V, 5 ms, twice or at 700 V, 5 milliseconds (ms), 10 times, with 30 s delay between pulses using Multiporator® electroporator (Eppendorf, Hamburg, Germany). After electroporation, the unencapsulated FAM-antimiR was separated using Size Exclusion Chromatography (SEC) over a Micro-Bio Spin® P-30 column (Bio-Rad, Hercules, CA) equilibrated with hypo-osmolar electroporation buffer, for 1 min at 1000 g. Samples were diluted in phosphate buffer saline (PBS) 1:100, added to a black 96 well plate (ThermoFisher Scientific, Waltham, MA) and FAM-fluorescent intensity was measured using VarioSkan™ Flash microplate reader (ThermoFisher Scientific, Waltham, MA). The amount of encapsulated antimiR was determined by interpolation with a standard curve. Encapsulation efficiency (EE) was calculated as follows in Eq. (1):

$$Encapsulation\ Efficiency\ (EE\%) = \frac{weight\ of\ the\ final\ amount\ of\ therapeutic}{weight\ of\ the\ initial\ amount\ of\ therapeutic} X100$$

To study the stability of antimiR during electroporation, a solution of FAM-antimiR-221 (100 nM) and electroporation buffer was electroporated in a 2-mm gap cuvette (Cell projects, Harrietsham, UK) at 2500 V, 5 ms, twice, or at 700 V, 5 ms, 10 times, with 30 s delay between pulses using Multiporator® electroporator (Eppendorf, Hamburg, Germany) (replicates >3). The stability of the fluorescent FAM tag and the charge after electroporation were assessed by VarioSkan™ Flash microplate reader (ThermoFisher Scientific, Waltham, MA) and by Zetasizer Nano-Series (Malvern Instruments, Malvern-Worcestershire, UK) (replicates = 3). antimiR aggregates were imaged by LSM700 laser scanning inverted confocal microscope (Zeiss, Oberkochen, Germany) using ZEN imaging software (Zeiss, Oberkochen, Germany). For the studies herein described, the concentration of encapsulated antimiRs is referred to as total molar (M) concentration of antimiRs that is entrapped in the NGs, based on the EE.

2.4. Release profile of antimiR-221 from NGs

FAM-AntimiR encapsulated-NGs (100 nM) or free FAM-antimiR (100 nM) were loaded in Slide-A-Lyzer™ MINI dialysis cups 10 K molecular weight cut-off (MWCO) (ThermoFisher Scientific, Waltham, CA). The dialysis cups were placed in Eppendorf with 900 μL of PBS and kept on gentle stirring (200 rpm) either at 4 °C or 37 °C for up to 48 h. The dialysate was sampled at specific time points (2, 4, 6, 24, and 48 h) and the NGs retained in the cups were collected at the endpoint; FAM-fluorescent intensity in the dialysates was measured using Varioskan™ Flash microplate reader (ThermoFisher Scientific, Waltham, MA) and FAM-antimiR concentration was determined against a standard curve (replicates >3).

2.5. NGs cellular uptake and antimiR-221 delivery

To test NGs cellular uptake, MSCs and SMCs were seeded at a density of $1\bullet10^5$ cells cm^{-2} in α-MEM medium and allowed to adhere overnight. The following day, the medium was refreshed using α-MEM medium containing DiD-NGs (5 μg mL^{-1}) or with only medium and incubated for 5, 15, and 30 min at 37 °C. At each time point, the medium was removed, the samples were washed twice with PBS, harvested with 0.05% trypsin, and resuspended in PBS (500 μL). All samples were analyzed by flow cytometry for DiD fluorescence using a FACSCalibur (BD™ Bioscience, San Diego, CA) as previously described [18,21]. Data were analyzed using FCS Express 4 software analysis (DeNovo Software, Pasadena, CA) (replicates >3). To test NGs internalization and antimiR delivery in the cytoplasm, MSCs were incubated with FAM-antimiR (100 nM) loaded DiD-NGs for 24 h. The medium was removed, the samples were washed twice with PBS, harvested with 0.05% trypsin, and analyzed by imaging flow cytometry using Amins® ImageStream®X Mark II (Luminex Corporation, Austin, TX). Data were obtained from a minimum of $1\bullet10^4$ cells per sample and analyzed using IDEAS software internalization wizard feature (Luminex Corporation, Austin, TX) (replicates = 3).

2.6. Intracellular trafficking of NGs

For live kinetic analysis of NGs intra-cellular trafficking, MSCs were seeded at a density of $1.5\bullet10^4$ cells cm^{-2} in a 96 wellplate in medium α-MEM medium and allowed to adhere overnight. Early endosomes (EE) and late endosomes (LE) were stained using CellLight™ Early or Late Endosomes-RFP, BacMam 2.0 (Life Technologies™, Carlsbad, CA) using a concentration of 50 particles per cell (ppc), according to the manufacturer's instructions. Cells were washed twice with PBS and lysosomes were labelled using LysoTracker™ DND-99 (70 nM) (Life Technologies™, Carlsbad, CA) for 30 min at 37 °C. Cells were washed twice, and nuclei were stained using Hoechst 33342 (5 μg mL^{-1}) (Sigma-Aldrich™, St. Louis, MO) for 20 min. Cells were washed twice with PBS and incubated with DiD-NGs (5 μg mL^{-1}) for 2 h. Cells were washed twice with PBS and fresh α-MEM medium was added. The 96 wellplate was incubated at 37 °C, 5% CO_2 inside InCell analyzer 2000 (General Electric, Boston, MA). Live kinetic was set, and each sample was imaged every 30 min for 17 h. Then, the images were analyzed using InCell Investigator software (replicates >3). To test NGs and antimiR co-localization with LE and lysosomes, MSCs were incubated with FAM-antimiR (100 nM) loaded NGs or DiD-NGs for 24 h. The medium was removed, the samples were washed twice with PBS, harvested with 0.05% trypsin, and analyzed by imaging flow cytometry using Amins® ImageStream®X Mark II (Luminex Corporation, Austin, TX). Data were obtained from a minimum of $1\bullet10^4$ cells per sample and analyzed using IDEAS software co-localization wizard feature (Luminex Corporation, Austin, TX) (replicates = 3).

2.7. Imaging of NGs internalization and antimiR-221 delivery

To study NGs internalization by the cells and delivery of antimiR-221, we conducted different imaging techniques. For confocal imaging of MSCs cultured in monolayer, $2\bullet10^4$ cells cm^{-2} were seeded in an optical bottom μ-Slide 8 well (Ibidi, Martinsried, Germany), in α-MEM medium and allowed to adhere overnight. The cells were incubated with DiD-NGs (5 μg mL^{-1}) for 24 h. For confocal imaging of MSCs cultured in the hydrogel or endogenous cells migrated *in vivo*, cells were released from the hydrogels by treatment with Collagenase B (2 mg mL^{-1}) (Sigma-Aldrich™, St. Louis, MO) for 90 min in an optical bottom 24 well plate (Ibidi, Martinsried, Germany), and the cells were allowed to adhere for 2 h at 37 °C. The samples were prepared for imaging by washing with PBS and fixing with Paraformaldehyde (PFA) 4% for 20 min at RT. Next, the cells were washed three times with PBS and permeabilized with 0.1% solution of PBS-Triton X-100 (Sigma-Aldrich™, St. Louis, MO) for 5 min and washed again three times with PBS. The permeabilized cells were incubated with phalloidin-TRITC (25 μg mL^{-1}) (Life Technologies™, Carlsbad, CA) for 60 min at RT, washed three times with PBS, and mounted using DAPI-Fluoromount-G® (Southeriotech, Birmingham, AL). Cells not incubated with NGs were utilized as negative control. Samples were imaged using an LSM700 laser scanning inverted confocal microscope (Zeiss, Oberkochen, Germany) and 63×/1.4 oil-immersion objective, and analyzed by ZEN imaging software (Zeiss, Oberkochen, Germany) and IMARIS image analysis software (Oxford Instruments, Abingdon, UK) (replicate >3). For late endosomes immunostaining, cells were fixed in 4% formalin for 10 min, followed by permeabilization with 0.1% PBS-Triton X-100 for 20 min. Blocking was performed using 5% PBS-BSA for 30 min followed by 1 h incubation at RT with anti-Rab7 (H4A3, DSHB) antibody (1.25 μg mL^{-1}) targeting LE. Subsequently, Alexa Fluor®488 goat anti-mouse (ThermoFisher Scientific, Waltham, MA) antibody (8 μg mL^{-1}) was added and incubated for 1 h at RT. Cells were counterstained with Phalloidin-TRITC (2.5 μg mL^{-1}) (Sigma-Aldrich™, St. Louis, MO) and DAPI (100 ng mL^{-1}) for 60 min. After each step, cells were washed three times with 0.05% PBS-Tween. Images were acquired using a Leica SP8X confocal microscope (Leica, Wetzlar, Germany) and 63×/1.4 oil-immersion objective. Images were analyzed by ZEN imaging software (Zeiss,

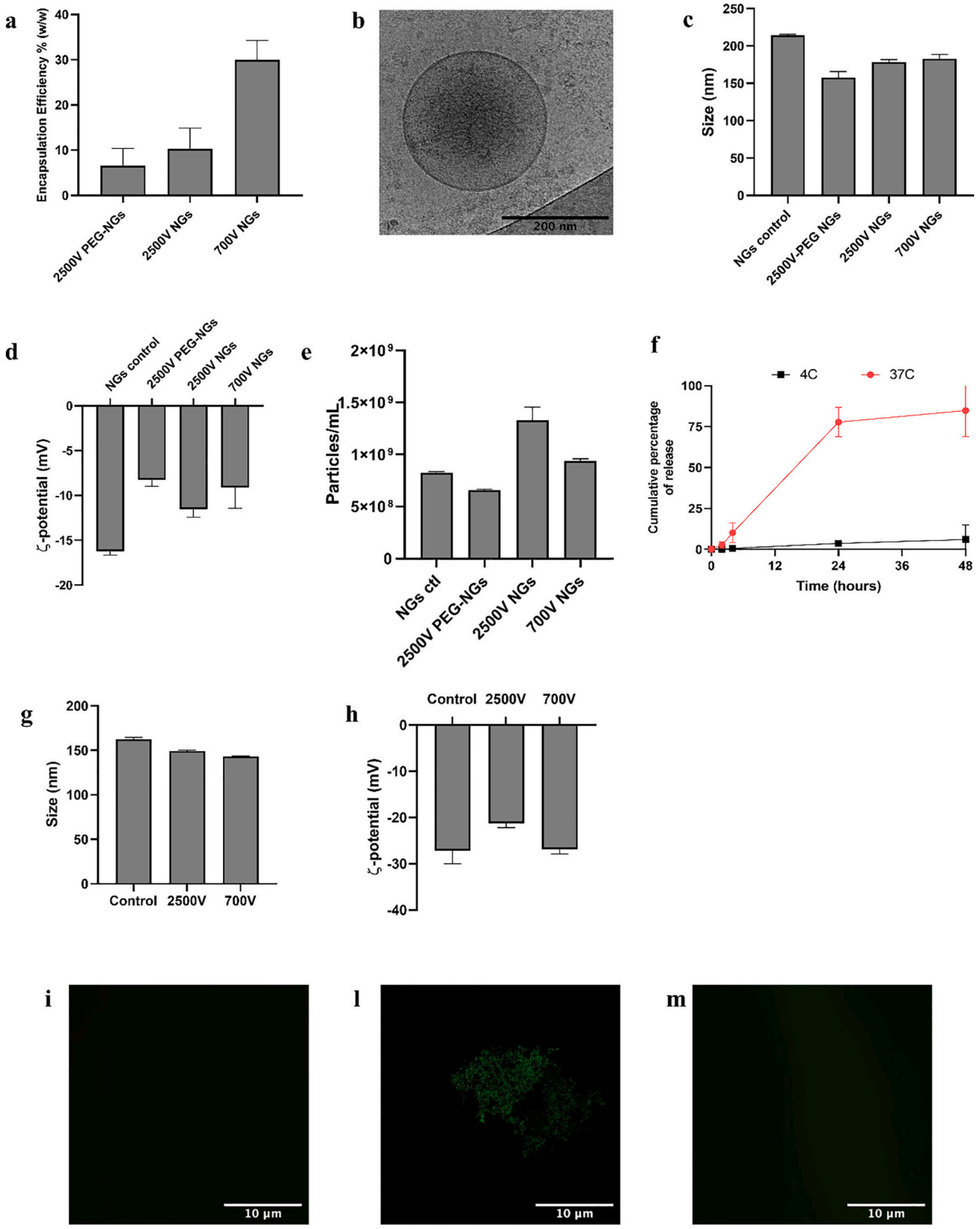

Fig. 1. AntimiR-221 loading of Nano-Ghosts (NGs) by electroporation and stability study. a) Electroporation settings tested for the optimization of 6-Carboxyfluorescein (6-FAM)-antimiR encapsulation into the NGs. b) Transmission electron cryomicroscopy (Cryo-TEM) microscopy images of antimiR-loaded NGs. c) Nanoparticle tracking analyzer (NTA) of control and antimiR-loaded NGs. d) Dynamic Light Scattering (DLS) analysis of surface ζ-potential of control and antimiR-loaded NGs. e) Particles concentration analyzed by nanoparticle tracking analyzer (NTA) of control and antimiR-loaded NGs. f) Release profile kinetics of antimiR-loaded NGs at 37 °C and 4 °C. g) Fluorescent intensity of antimiR 6-FAM tag of control and electroporated antimiR. h) Dynamic Light Scattering (DLS) analysis of the charge of control and electroporated FAM-antimiR. i),l),m) Confocal microscopy images of buffer only (i), FAM-antimiR 2500 V (l) and FAM-antimiR 700 V (m).

Oberkochen, Germany) and IMARIS image analysis software (Oxford Instruments, Abingdon, UK) (replicates >3).

2.8. Cryo TEM analysis of NGs characterization and antimiR encapsulation

NGs morphology was assessed using T12 G2-Transmission electron microscopy, Cryo-TEM (FEI, Hillsboro, OR) operated at 120 kV. Cryo-TEM images were recorded on a Gatan US1000 2 k × 2 k high-resolution cooled CCD camera using Digital Micrograph software. Samples for Cryo-TEM imaging were prepared as previously published. [26]

2.9. MSCs viability and proliferation

To study the effect of NGs and NGs loaded with antimiR on cell viability, MSCs were seeded at a density of $2\bullet10^4$ cells cm^{-2} in α-MEM medium and allowed to adhere overnight. The medium was refreshed with medium containing NGs-antimiR-221 (100 nM), NGs-antimiR-Scr (100 nM), or empty NGs (μg of phospholipids equivalent to encapsulated NGs), and incubated for 24, 48, and 72 h. At each time point, a viability assay was performed by Propidium Iodide (PI) assay (replicates = 3) and the proliferation rate of MSCs was determined by AlamarBlue™ assay (replicates >3) (Bio-Rad, Hercules, CA), according to the manufacturer's instructions. For PI viability assay, cells were harvested with 0.05% trypsin at each time point, centrifuged at 300 *g*, and resuspended in PBS (500 μL). The flow cytometer settings were adjusted using PI staining solution (5 μL) to a control tube of otherwise unstained cells. PI staining solution (5 μL) was added to each sample just prior to the analysis. Samples were measured using a FACSCalibur™ (BD™ Bioscience, San Diego, CA), and data were analyzed using FCS Express 4 software analysis (DeNovo Software, Pasadena, CA). For the proliferation assay, cells were incubated for 4 h with AlamarBlue™, and the supernatant was added to a 96 well plate. The visible light absorption was determined at 530 and 590 nm by a Varioskan™ Flash microplate reader (ThermoFisher Scientific, Waltham, MA).

2.10. In vitro transfection of MSCs cultured in 2D

For the *in vitro* miR-221 silencing studies, MSCs were seeded at a density of $2.5\bullet10^4$ cells cm^{-2} in α-MEM medium and allowed to adhere overnight. Then, the cells were transfected with antimiR-221 or antimiR-Scr loaded NGs (25 or 50 nM), or antimiR-221 loaded Lipofectamine RNAiMAX reagent (ThermoFisher Scientific, Waltham, MA) (3 replicates for 2 donors). The transfected cells were cultured for 24 and 72 h, at 37 °C in a humidified atmosphere of 5% CO_2.

2.11. Hydrogel preparation and MSCs culture

The HA-FB conjugate hydrogel (RegenoGel™ ProCore Biomed Ltd. Nes Ziona, Israel). The hydrogel is composed of FB (6.25 mg mL^{-1}) and HA (1.95 mg mL^{-1}). HA-FB hydrogel constructs for *in vitro* cultures were prepared by mixing HA-FB hydrogel (100 μL) with thrombin (10 μL of 50 U mL^{-1}) (Sigma-Aldrich™, St. Louis, MO). The hydrogels were polymerized at 37 °C for 30 min in 96 well plate, removed from the plate, and used for the different experiments. When necessary, MSCs ($2\bullet10^5$ cells per hydrogel) were resuspended in the hydrogel prior to the addition of thrombin. To prepare NGs-antimiR hydrogels, HA-FB was loaded with the indicated concentrations of antimiRs prior to polymerization (replicates = 3 for both inhibitors tested). For positive transfection controls, Lipofectamine RNAiMAX Reagent (ThermoFisher Scientific, Waltham, MA) was used as transfecting agent and pre-incubated with the indicated concentration of antimiR and Opti-MEM Reduced Serum Medium (ThermoFisher Scientific, Waltham, MA) for 20 min at RT, following the manufacturer's instructions, prior to addition to the hydrogels.

2.12. RNA isolation and quantitative real-time polymerase chain reaction analysis

Total RNA, including miRNAs, was extracted from MSCs cultured in monolayer using the RNeasy Plus Micro Kit (Qiagen, Hilden, Germany), according to the manufacturer's instructions. For RNA extraction from hydrogels, they were manually homogenized in QIAzol Lysis Reagent (700 μL) (Qiagen, Hilden, Germany) and total RNA including miRNAs was purified using the miRNeasy Micro Kit (Qiagen, Hilden, Germany). RNA concentration was measured using NanoDrop 2000c (ThermoFisher Scientific, Waltham, MA). cDNA was synthesized from a total RNA (300 ng) using TaqMan™ MicroRNA Reverse Transcription Kit (ThermoFisher Scientific, Waltham, MA) according to manufacturer's instructions for miRNAs-specific amplification. The quantification of hsa-miR-221-3p was performed using the TaqMan™ microRNA assay (ThermoFisher Scientific, Waltham, MA) and using small ribonucleic RNA (snRNA) U6 as normalization control. Quantitative PCR was performed using TaqMan™ fast advance master mix (ThermoFisher Scientific, Waltham, MA) or TaqMan™ Universal PCR Master mix (ThermoFisher Scientific, Waltham, MA) and using CFX96TM PCR detection system (Bio-Rad, Hercules, CA) or QuantStudio 12 K Flex Real-Time PCR System (ThermoFisher Scientific, Waltham, MA). Relative gene expression was calculated using the comparative $2^{-\Delta Ct}$ method.

2.13. In vivo osteochondral biopsy model for NGs-mediated delivery of antimiR to endogenous cells

Osteochondral biopsies that were 8 mm in diameter and 4 mm in height were produced with a drill from the metacarpal bones of fresh metacarpal-phalangeal joints of 3 to 8 month-old calves obtained from the slaughterhouse. Using a 4 mm-diameter dermal biopsy punch (Stiefel Laboratories, Germany) and a scalpel, osteochondral defects were created by removing the cartilage and part of the subchondral bone. The specimens were incubated overnight in α-MEM medium supplemented with 10% FCS, Fungizone™ (1.5 μg mL^{-1}), and gentamicin (50 μg mL^{-1}) to verify sterility. All defects were filled with lipofectamine-antimiR (100 nM), or NGs-antimiR (500 nM). The osteochondral biopsies were covered using an 8 mm diameter Neuro-Patch membrane (Braun, Melsungen, Germany) to prevent in-growth of host cell/tissue. The osteochondral biopsies were implanted subcutaneously on the back of 10–14-week-old female NMRI nu/nu mouse (Charles River, Wilmington, MA) under isoflurane anesthesia (2 replicates for 3 mice). Before surgery and 6 h after surgery, mice received Temgesic (0.05 mg kg^{-1}) (Reckitt Benckiser, Slough, U.K.) During surgery, mice received Ampidry (9 mg kg^{-1}) (Dopharma, Raamsdonksveer, The Netherlands). After 7 and 14 days, mice were euthanized by cervical dislocation, and the osteochondral biopsies were explanted, hydrogels were removed from the defects using a sterile spatula and processed as previously described in paragraph 2.10. Animal experiments were conducted in the animal facility of the Erasmus MC with approval of the animal ethics committee (license AVD101002016691, protocol 16–691-04).

2.14. Statistical analysis

Results are presented as the mean ± SD (standard deviation) of at least triplicates. The normal distribution of data was verified using the Kolmogorov-Smirnov test. For single comparison, statistical significance was analyzed by Student's *t*-test; for multiple comparisons, statistical significance was analyzed by ANOVA and Tukey *post hoc* test. Differences were considered as statistically significant for *p*-values ≤ 0.05.

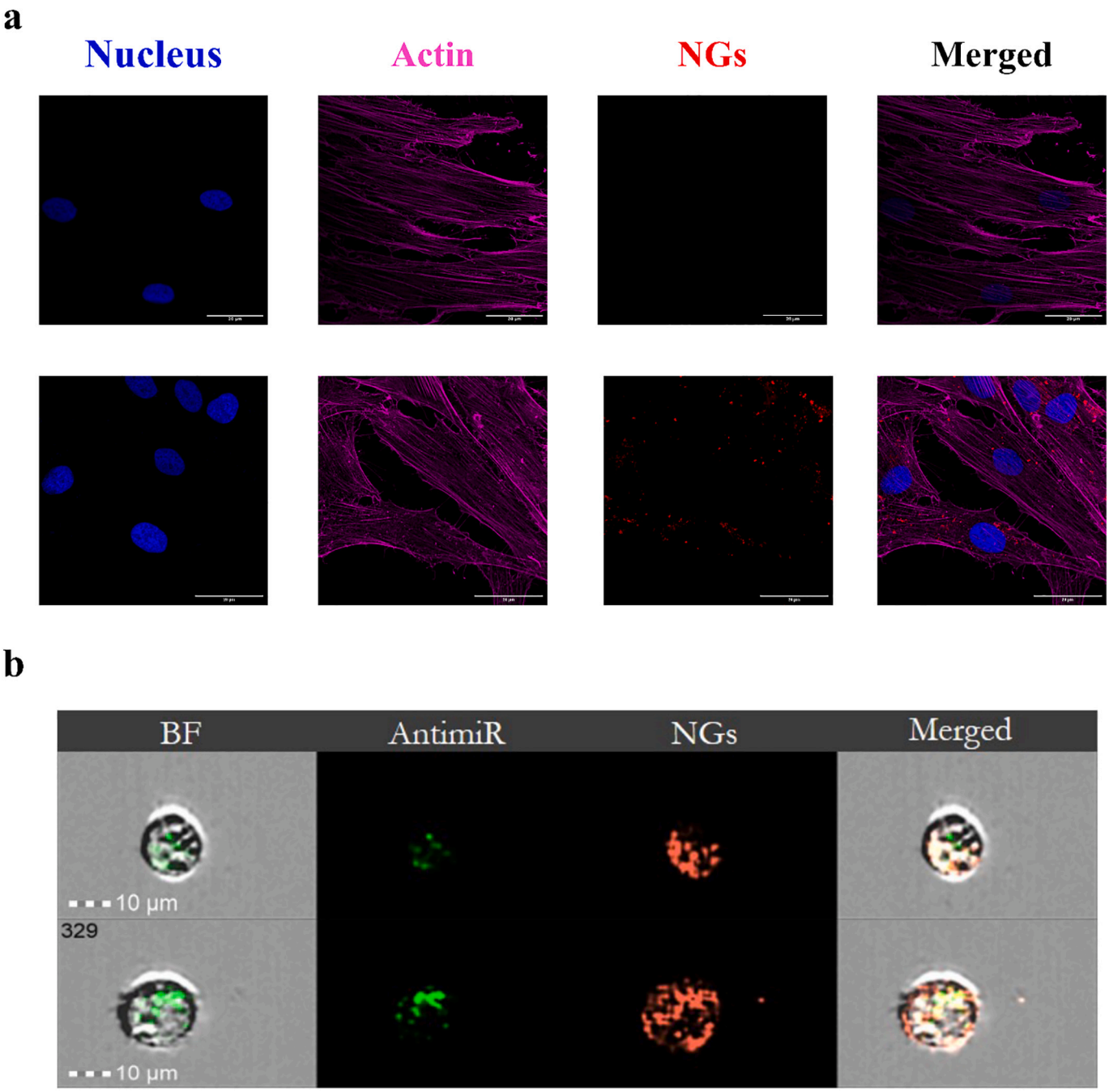

Fig. 2. Nano-Ghosts (NGs) internalization in Mesenchymal Stem Cells (MSCs) and deliver antimiR-221 intracellularly. a) Confocal microscopy images of control MSCs and MSCs incubated with fluorescently labelled NGs for 24 h (Nucleus – 4′,6-diamidino-2-phenylindole (DAPI), Actin – Phalloidin-Tetramethylrhodamine (TRITC), NGs–3,3'-Dioctadecyloxacarbocyanine Perchlorate-(DiO). b) Imaging flow-cytometry (ImageStream®X Mark II) analysis of fluorescently labelled NGs internalization in and antimiR delivery to MSCs (AntimiR – 6-Carboxyfluorescein (6-FAM), NGs –1,1'-Dioctadecyl-3,3,3′,3'-Tetramethylindodicarbocyanine Perchlorate(DiD)).

3. Results

3.1. Electroporation-based encapsulation results in efficient loading of antimiR into the NGs

The effect of different electroporation parameters was addressed to achieve antimiR loading into the NGs as well as to evaluate the stability of NGs and antimiR undergoing the electroporation process (Fig. 1). High voltage (2500 V) conditions with 2 pulses and the presence of PEG resulted in an encapsulation efficiency (EE) of 6.54 ± 3.84%, and performing electroporation prior to NGs PEGylation with 10 pulses resulted in 10.32 ± 4.56% EE (Fig. 1a). Using low voltage conditions (700 V) and performing the electroporation prior to NGs PEGylation, significantly increased the EE up to 30 ± 4.29% (Fig. 1a). The integrity of the loaded particles was confirmed by Cryo-TEM imaging (Fig. 1b and Fig. S1). The nano-vesicles were stable after the electroporation process as demonstrated by negligible variations in vesicle size (Fig. 1c), ζ-potential (Fig. 1d) and particles concentration (Fig. 1e). Unaltered fluorescent intensity of the 5'-FAM tag indicated stability of the antimiR after electroporation (Fig. 1g). Furthermore, the charge of the FAM-tagged antimiR was not affected by low voltage electroporation (Fig. 1h) and only the high voltage conditions led to antimiR aggregation (Fig. 1i-m).

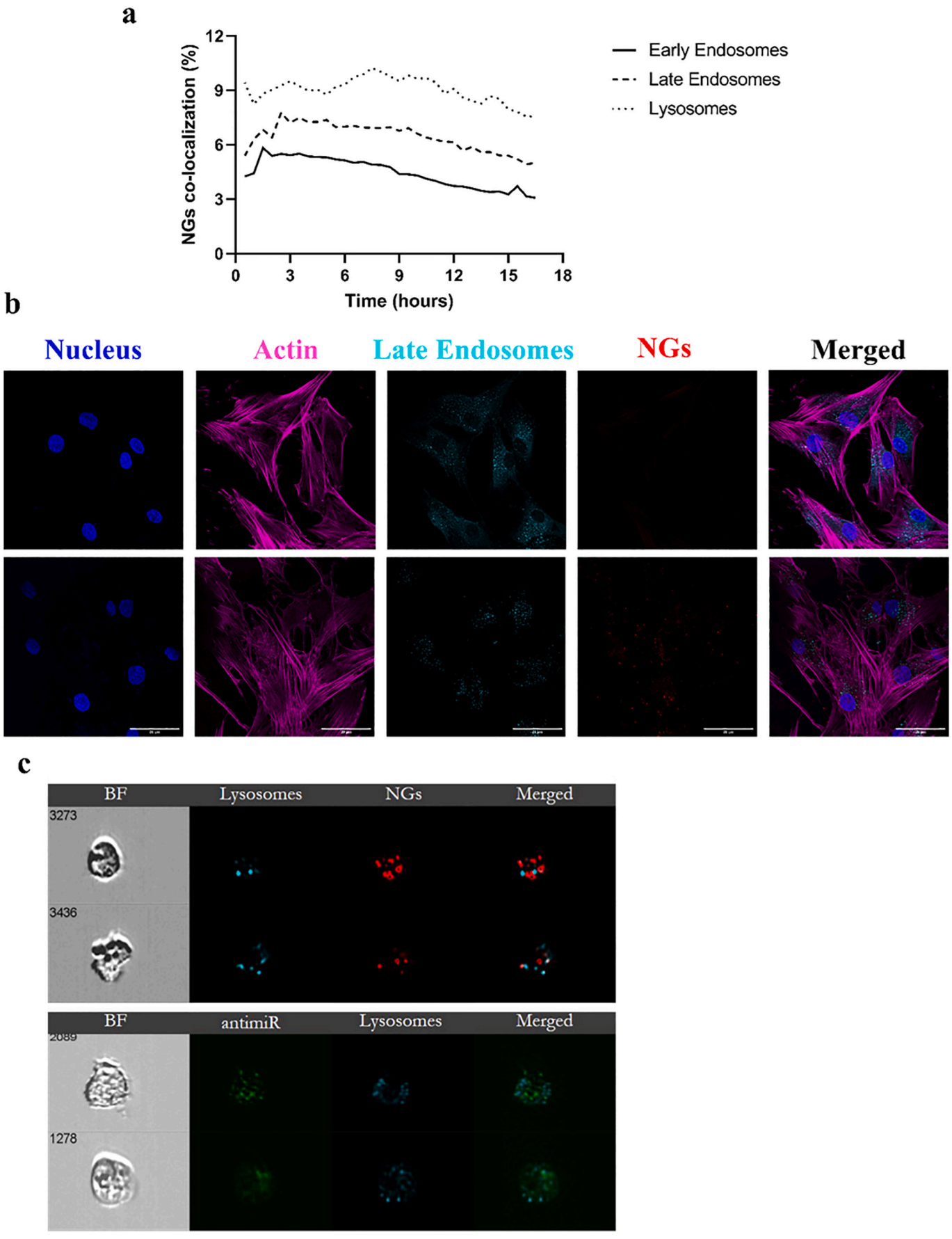

(caption on next page)

Fig. 3. Nano-Ghosts (NGs) intra-cellular trafficking. a) *In vitro* High Content Analysis (HCS) live kinetics of fluorescently labelled NGs co-localization with early endosomes (EE), late endosomes (LE) and lysosomes in mesenchymal stem cells (MSCs). b) Confocal microscopy images of fluorescently labelled NGs co-localization with LE (6.22% co-localization) (Nucleus – Hoechst 33342 or 4′,6-diamidino-2-phenylindole (DAPI), Actin – Phalloidin- Tetramethylrhodamine (TRITC), late endosomes – AlexaFluor®488, NGs– 1,1'-Dioctadecyl-3,3,3′,3'-Tetramethylindodicarbocyanine Perchlorate (DiD)). c) Imaging flow-cytometry (ImageStream®X Mark II) analysis of fluorescently labelled NGs and antimiR co-localization with lysosomes (1.2% and 1.1%, respectively) (AntimiR – 6-FAM, NGs – DiD, lysosomes – Lysotracker DND-99).

Based on these results, we selected the 700 V voltage settings and post-encapsulation PEGylation as conditions for the following experiments.

In addition, to investigate whether the NGs retained antimiR after the encapsulation, the release profile of antimiR from the NGs was studied at 4 °C and 37 °C, at different time points up to 48 h (Fig. 1f). Two distinct profiles were observed, indicating that only at 37 °C there was a substantial release of antimiR from the NGs over time, while at 4 °C, considered as storage temperature, there was only a minimal release of antimiR. Taken together, our data indicate that electroporation can be employed as an effective method to encapsulate antimiR ASOs into the NGs.

3.2. NGs are efficiently internalized by MSCs and deliver the antimiR payload intracellularly

The uptake of the NGs in MSCs, their efficiency in delivering the antimiR cargo and their intracellular trafficking were investigated *in vitro*. Confocal microscopy analysis of MSCs, 24 h post transfection, with fluorescently labelled DiO-NGs demonstrated uptake of NGs in MSCs (Fig. 2a). Quantification analysis of *Z*-stack images revealed that >90% of NGs were localized inside the cells rather than on the cell surface (Video S2a). Flow cytometry analysis confirmed the NGs internalization at early time points (5, 15, and 30 min post incubation with NGs, Fig. S3b); NGs were preferentially internalized by MSCs over smooth muscle cells (SMCs) used as control, already as early as 15 min post incubation. NGs internalization in MSCs and effective antimiR delivery were confirmed at 24 h post NGs incubation. Imaging flow cytometry (ImageStream), indicated that 87% and 80% of the cells were DiD-NGs and FAM-antimiR positive, respectively (Fig. 2b).

Once internalized by the cells, NGs exhibited minimal co-localization with early endosomes (peak of 5.82% after 1.5 h), late endosomes (peak of 7.76% after 2.5 h) and lysosomes (peak of 10.22% after 7.5 h) along with a decreasing trend of co-localization over the time, as demonstrated by live kinetic High Content Screening (HCS) (Fig. 3a). In line with these data, immunofluorescence imaging analysis confirmed a low NGs co-localization with late endosomes (6.22%) (Fig. 3b). Finally, MSCs were incubated with antimiR-loaded NGs to verify whether the antimiR delivered by the NGs was degraded by the lysosomes and whether the encapsulation process affected the trafficking of the NGs. The ImageStream analysis showed that NGs and FAM-antimiR delivered by DiD-NGs were only minimally co-localized with lysosomes (1.2 and 1.1%, respectively) (Fig. 3c). Collectively, these data demonstrate the efficacy of the NGs uptake by MSCs and delivering their cargo in the cytoplasm avoiding *endo*-lysosomal degradation.

3.3. NGs-antimiR strongly inhibit miR-221 expression in MSCs

We next aimed to address the question of whether the antimiR delivered by NGs could suppress miR-221 expression in MSCs. First, the effect of NGs-antimiR on MSC viability and proliferation and miR-221 expression was studied in monolayer. NGs alone or loaded with antimiR or antimiR-Scr did not affect MSC viability and proliferation up to 72 h (Fig. 4a). miR-221 expression was strongly reduced at both 24 h and 72 h post-incubation, and for different concentrations of NG-antimiR (25 and 50 nM), with ~90% inhibition at 72 h (Fig. 4b). Incubation of MSCs with NGs-AntimiR-Scr did not affect miR-221 expression, indicating specific inhibition of miR-221 by NGs-antimiR. Altogether, these data demonstrate the effectiveness of the NGs as delivery system for antimiR ASOs *in vitro*.

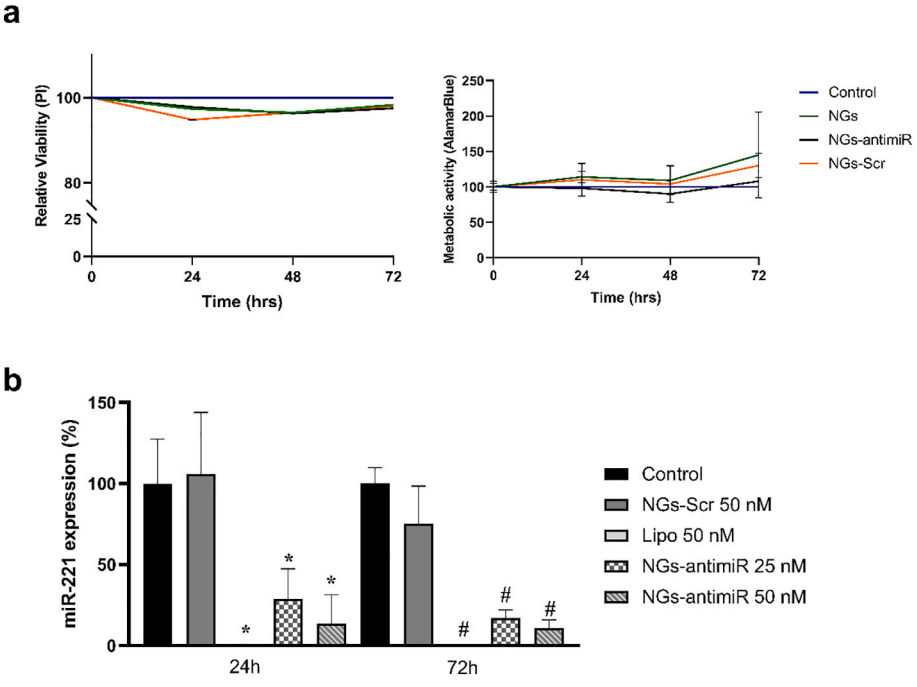

Fig. 4. *In vitro* mesenchymal stem cells (MSCs)' viability, proliferation and 2D miR-221 silencing. a) Flow cytometry Propidium iodide (PI) study of MSCs viability and AlamarBlue metabolic assay of MSCs proliferation when incubated with Nano-Ghosts only (NGs), antimiR-scramble loaded NGs (antimiR-Scr-NGs) or antimiR-221 loaded NGs (antimiR-NGs) compared to untreated cells (Control). b) qPCR analysis of 2D *in vitro* miR-221 expression at 24 and 72 h post-transfection with antimiR-scramble loaded NGs (NGs-Scr), antimiR-221 loaded NGs (antimiR-NGs) or Lipofectamine antimiR-221 (Lipo-antimiR). Lipofectamine was used as positive control for transfection. Statistical significance in the differences of the means was evaluated by ANOVA and Tukey *post hoc* test. * $p < 0.05$ compared to control 24 h; # $p < 0.05$ compared to control 72 h.

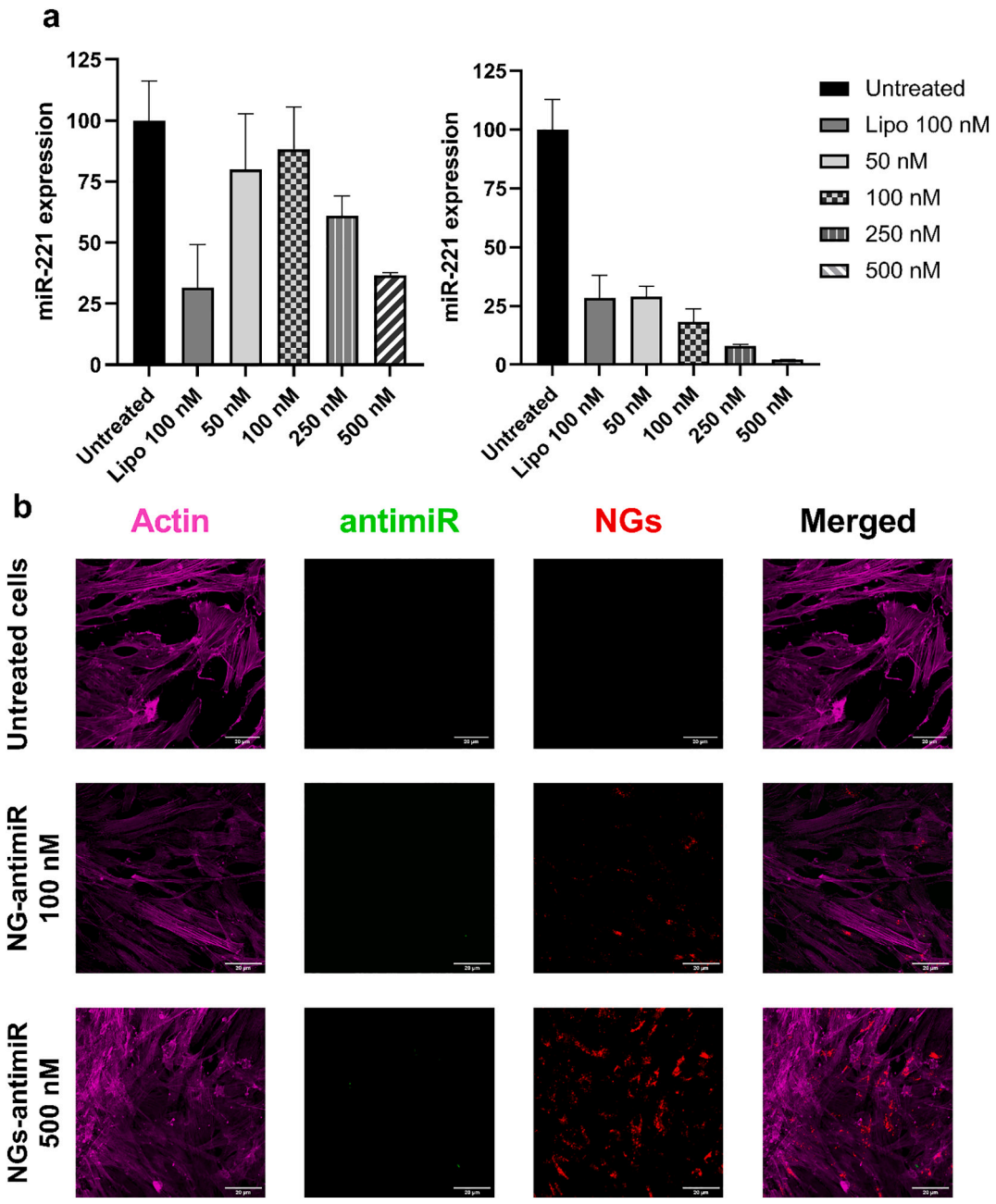

Fig. 5. miR-221 silencing in hyaluronic acid-fibrin (HA-FB) 3D *in vitro* cell culture. a),b) Quantitative PCR (qPCR) analysis of miR-221 expression in MSCs after 7 days of 3D HA-FB culture with different doses of antimiR (a) or Power-antimiR (b) loaded NGs; expression percentage is reported relative to untreated control cells. c) Confocal microscopy images of fluorescently labelled 6-Carboxyfluorescein (6-FAM)-Power-antimiR (100 or 500 n_M) loaded 1,1'-Dioctadecyl-3,3,3′,3'-Tetramethylindodicarbocyanine Perchlorate (DiD)-NGs uptake by mesenchymal stem cells (MSCs) after 7 days of 3D HA-FB culture (Actin – Phalloidin- Tetramethylrhodamine (TRITC), Power-antimiR – 6-FAM, NGs –3,3'-Dioctadecyloxacarbocyanine Perchlorate-(DiO). Cells were extracted from the HA-FB hydrogel before being processed for staining.

3.4. Loading of a HA-FB hydrogel with NGs-antimiR leads to effective miR-221 silencing in 3D culture and internalization by endogenous cells in vivo

We next investigated the possibility of combining the NGs with a scaffold system for potential applications in regenerative medicine. For this purpose, we exploited a HA-FB hydrogel that can sustain cells and NGs at the site of delivery, minimizing particle loss and potentially allowing for long term, local delivery of antimiR by the NGs. Since an *in vivo* approach of hydrogel-mediated transfection can pose significant challenges for transfection, we compared two inhibitors presenting differences in chemical modifications (AntimiR and Power-AntimiR) and a range of concentrations (50 to 500 nM), to select the most effective strategy. NGs-antimiR or NGs-Power-antimiR and MSCs were loaded in HA-FB hydrogels and cultured *in vitro* for 7 days. Both antimiR molecules repressed the expression of miR-221 in MSCs embedded in the hydrogel (Fig. 5 a and b). The Power-antimiR showed a stronger dose-dependent silencing effect at all concentrations tested, (50–500 nM), reaching a 98% miR-221 knockdown efficiency for 500 nM Power-antimiR (Fig. 5b). Remarkably, the NGs-mediated delivery of Power-antimiR had a comparable effect to the use of a state-of-the-art liposomal carrier (Lipofectamine, Fig. 5b). Confocal microscopy imaging further confirmed effective NGs-mediated delivery of Power-antimiR to MSCs in HA-FB hydrogel for different Power-antimiR concentrations

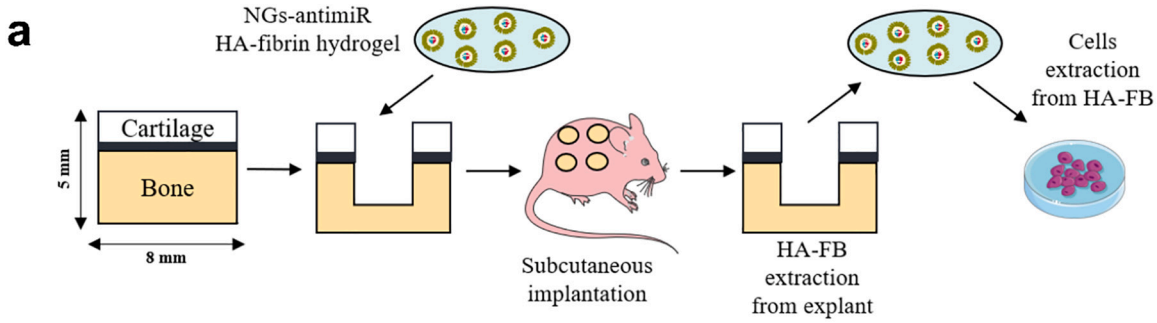

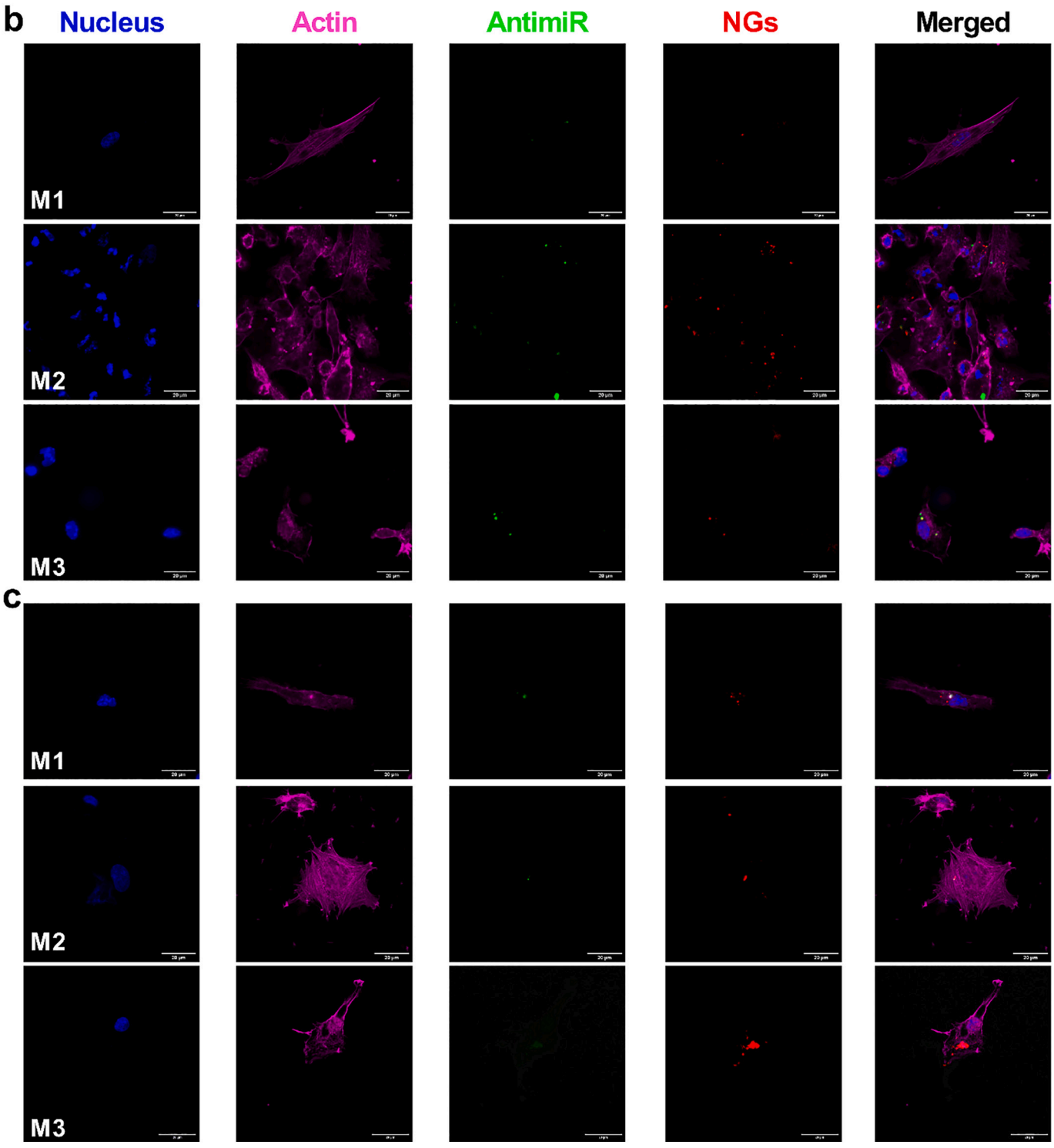

(caption on next page)

Fig. 6. *In vivo* Nano-Ghosts-mediated delivery of antimiR to endogenous cells. a) Schematic representation of the osteochondral defect model. b),c) Confocal microscopy images of fluorescently labelled 6-Carboxyfluorescein (6-FAM)-Power-antimiR (500 nM) loaded 1,1'-Dioctadecyl-3,3,3′,3'-Tetramethylindodicarbocyanine Perchlorate (DiD)-NGs internalized in endogenous cells that infiltrated the cartilage defect after 7 (b) and 14 (c) days; each image represents a sample from a different animal of 7 and 14 days group, respectively (Nucleus – 4′,6-diamidino-2-phenylindole (DAPI), Actin – Phalloidin-Tetramethylrhodamine (TRITC), Power-antimiR – 6-FAM, NGs– DiD). Cells were extracted from the hyaluronic acid-fibrin (HA-FB) hydrogel before being processed for staining. The schematic art pieces used in this figure were provided by Servier Medical art (https://smart.servier.com/). Servier Medical Art by Servier is licensed under a Creative Commons Attribution 3.0 Unported License.

(100 and 500 nM, Fig. 5c). Based on these results, the Power-antimiR was selected as ASO for the following *in vivo* study.

Finally, to study the effectiveness of the NGs as a delivery system for antisense oligonucleotides *in vivo*, we tested their ability to deliver antimiR-221 to endogenous cells *in situ* using an osteochondral defect model (Fig. 6a). Using this model, we previously showed the ability of endogenous cells to infiltrate the HA-FB hydrogel over time. [25,27] Osteochondral defects were created in bovine osteochondral plugs and filled with HA-FB hydrogel containing NGs-Power-antimiR, prior to subcutaneous implantation in mice (Fig. 6a). After 7 and 14 days, the constructs were retrieved and endogenous cells that had infiltrated the hydrogel were isolated by enzymatic digestion. Quantification analysis of confocal microscopy images showed the presence of NGs in the endogenous cells that had invaded the hydrogel (Fig. 6 b and c). Within the fields imaged for the quantification analysis, the majority of the NGs (97% after 7 days and 69% after 14 days) and of the power-antimiR (95% after 7 days and 62% after 14 days) was localized intracellularly in endogenous cells, while the rest was localized in the cells' outer membrane. In conclusion, the NGs could safely and efficiently delivery antimiR both to cultured and endogenous cells, demonstrating the possibility to apply the system for *in vivo* delivery. Moreover, the system was successfully integrated with a scaffold system, that could expand future therapeutic applications.

4. Discussion

With the discovery of miRNAs and the new therapeutic approaches of gene modulation at transcriptional level, the development of ASOs has grown exponentially, with six different classes of ASO molecules being now widely utilized. [28] However, this has not been equally followed by the design of safe, targeted, and suitable delivery systems. Since the first delivery system proposed by Loke et al. [29], many have been investigated, but only one oligonucleotide-liposomal formulation (Patisiran) has been approved for clinical use in 2018. [30] Among the development of many nano-carrier systems, exosomes have attracted attention for their natural origin and high intercellular communication properties; their natural characteristics of small RNAs transport have been exploited to develop them as new ASOs delivery system. [31] Nevertheless, the heterogeneity, poor characterization, and difficulties in scaling up production may hamper the exosomes' development as a suitable delivery system. [16] Here, for the first time, we demonstrated that our NGs platform is a new efficient delivery system for ASOs, using an antimiR molecule as proof-of-principle. The NGs unique properties and the efficient and tunable encapsulation method here presented, open to possible novel therapeutic approaches using the NGs-ASOs platform for several diseases. In parallel, for the first time, we have shown the successful integration of NGs with a hydrogel scaffold that provides a further novel level of applicability to the NGs-ASOs platform in regeneration medicine and tissue engineering.

NGs are empty vesicles produced by a scalable mechanical process and they can be utilized as a delivery system for different payloads [19]. The NGs retention of MSCs membrane markers and features renders them biocompatible and entails them with targeting properties thus avoiding the need for major and complicated modifications as it has been demonstrated by our group. [18,21] As MSCs play a major role in regenerative medicine strategies we here demonstrated the ability of the NGs to target MSCs *in vitro*.

The majority of nanocarriers are known to be internalized by the cells and degraded at different stages by the *endo*-lysosomal system, failing to deliver their cargo in the cytoplasm. [15,28] The 'proton sponge effect' [32] and the flipping mechanism [33] caused by polycationic polymers and cationic nanoparticles, respectively, are two examples of strategies developed to promote the endosomal escape. Biomimetic approaches have shown the tendency to avoid the degradation by lysosomes [34]; in line with this evidence, the NGs exhibited only a minimal co-localization with the endo-lysosomal compartment, which may be attributed to the retention of MSCs' surface markers that prevent the NGs to undergo degradation through the lysosomes. Moreover, the strong knockdown of miR-221 induced by antimiR when delivered by the NGs confirms its release in the cytoplasm as well as the retention of its biological activity.

As the loading of ASOs in NVs has been challenging, many different methodologies have been tested. [35] Among them, electroporation has shown efficacy in loading nucleic acids in different types of NVs [31,36] as well as for pDNA in the NGs, as we previously published. [21] Since electroporation can alter particles properties and ASOs [37], we have tuned the settings to avoid the aggregation and to maximize the loading of antimiR in the NGs without altering the NGs properties. Only a slight reduction of ζ-potential was shown, remaining within the neutral range (±30 mV) [38] and without causing any changes to the NGs and their markers as previously demonstrated by us. [19,22] Noteworthy, the tunable encapsulation method and the similarity in the chemical structures of the different ASOs, might facilitate the encapsulation of other ASOs in NGs for new delivery applications.

To demonstrate the broad possibilities of NGs applications for tissue repair, we have studied their use as a stand-alone delivery system as well as the possibility to use them for the delivery of ASOs or factors in an engineered hydrogel scaffold for future tissue engineering applications. The combination of nanocarriers and scaffolds has been investigated over the years in several fields. [39–42] Here, we have shown that the integration of the NGs with HA-FB hydrogel enabled uptake of endogenous cells *in vivo*. The hydrogel used was Regenogel™, a hydrogel that previously showed positive results in cartilage defect models [43] and it is clinically proved in Israel as a treatment to relieve pain in osteoarthritis patients [44] and it is approved in Israel for osteoarthritis treatment. Moreover, this hydrogel was previously used to deliver antimiR-221 using lipofectamine as a carrier system [45]. In the current work, *in vitro* studies of the integration of antimiR-loaded NGs with HA-FB hydrogel revealed that the NGs retain their properties, and they successfully deliver antimiR to MSCs leading to knockdown of miR-221 expression after one week of 3D culture. Following *in vivo* studies in an osteochondral defect model using antimiR-NGs in combination with HA-FB hydrogel, we demonstrated the ability of the NGs to transfect the endogenous cells that infiltrated the hydrogel, and to deliver the antimiR already 7 and 14 days post-implantation. Retention of drugs *in situ* is a challenge [46–49] and our results indicate that the NGs can successfully work as a delivery system for antimiRs or other ASOs. Moreover, the flexibility of the NGs as a stand-alone delivery system or in combination with a scaffold or hydrogel, expands the uses they can be employed for.

5. Conclusions

In conclusion, using antimiR-221 as a proof-of-concept ASO molecule we have shown, for the first time, the efficiency and versatility of our unique biomimetic NVs as a delivery system that can be employed

for a wide range of drug delivery applications for ASOs therapy and regeneration medicine. Moreover, the additional novel approach of NGs combination with a hydrogel scaffold presented here can lead the way for a more universal integrated use of nano-carriers and scaffolds for several therapeutic applications.

Supplementary data to this article can be found online at https://doi.org/10.1016/j.jconrel.2021.03.018.

Credit author statement

All the authors contributed equally to this research.

Declaration of Competing Interest

The author M.M. is the inventor of a patent owned by the Technion Research and Development Foundation Ltd. (a subsidiary of the Technion IIT) entitled "liposomal compositions and uses of same" that includes concepts presented here and which was granted in the US (US 9,642,817 B2) and the EU (EP 2470164 B1), and which is pending registration in China (CN 102596179) and India (484/ MUMNP/2012). Prof. Avner Yayon is CEO of ProCore Bio Med Ltd. that commercializes the FB/HA hydrogel (FB/HA; RegenoGel™) used in this work. The other authors have no conflict of interest.

Acknowledgments

This work was supported by the European Union's Horizon 2020 research and innovation program under Marie Sklodowska Curie grant agreement No. 642414. The authors wish to thank Dr. Nitsan Dahan and Dr. Yael Lupu-Haber for assistance in microscopy and high content analysis studies.

References

[1] R.L. Setten, J.J. Rossi, S. Ping Han, The current state and future directions of RNAi-based therapeutics, Nat. Rev. Drug Discov. 18 (2019) 421–446, https://doi.org/10.1038/s41573-019-0017-4.
[2] A.M. Quemener, L. Bachelot, A. Forestier, E. Donnou-Fournet, D. Gilot, M.-D. Galibert, The powerful world of antisense oligonucleotides: From bench to bedside, Wiley Interdiscip. Rev. RNA (2020), https://doi.org/10.1002/wrna.1594 e1594.
[3] T.C. Roberts, R. Langer, M.J.A. Wood, Advances in oligonucleotide drug delivery, Nat. Rev. Drug Discov. (2020) 1–22, https://doi.org/10.1038/s41573-020-0075-7.
[4] G. Gibson, H. Asahara, microRNAs and cartilage, J. Orthop. Res. 31 (2013) 1333–1344, https://doi.org/10.1002/jor.22397.
[5] A. Lolli, L. Penolazzi, R. Narcisi, G.J.V.M. van Osch, R. Piva, Emerging potential of gene silencing approaches targeting anti-chondrogenic factors for cell-based cartilage repair, Cell. Mol. Life Sci. 74 (2017) 3451–3465, https://doi.org/10.1007/s00018-017-2531-z.
[6] R. Rupaimoole, F.J. Slack, MicroRNA therapeutics: towards a new era for the management of cancer and other diseases, Nat. Rev. Drug Discov. 16 (2017) 203–222, https://doi.org/10.1038/nrd.2016.246.
[7] E. Van Rooij, E.N. Olson, MicroRNA therapeutics for cardiovascular disease: opportunities and obstacles, Nat. Rev. Drug Discov. 11 (2012) 860–872, https://doi.org/10.1038/nrd3864.
[8] Y. Li, K.V. Kowdley, MicroRNAs in common human diseases, Genomics, Proteomics Bioinforma 10 (2012) 246–253, https://doi.org/10.1016/j.gpb.2012.07.005.
[9] C.M. Curtin, I.M. Castaño, F.J. O'Brien, Scaffold-based microRNA therapies in regenerative medicine and cancer, Adv. Healthc. Mater. 7 (2018) 1700695, https://doi.org/10.1002/adhm.201700695.
[10] E. van Rooij, S. Kauppinen, Development of microRNA therapeutics is coming of age, EMBO Mol. Med 6 (2014) 851–864, https://doi.org/10.15252/emmm.201100899.
[11] P. Barata, A.K. Sood, D.S. Hong, RNA-targeted therapeutics in cancer clinical trials: current status and future directions, Cancer Treat. Rev. 50 (2016) 35–47, https://doi.org/10.1016/j.ctrv.2016.08.004.
[12] R.L. Juliano, The delivery of therapeutic oligonucleotides, Nucleic Acids Res. 44 (2016) 6518–6548, https://doi.org/10.1093/nar/gkw236.
[13] S.F. Dowdy, Overcoming cellular barriers for RNA therapeutics, Nat. Biotechnol. 35 (2017) 222–229, https://doi.org/10.1038/nbt.3802.
[14] J.C. Kaczmarek, P.S. Kowalski, D.G. Anderson, Advances in the delivery of RNA therapeutics: from concept to clinical reality, Genome Med. 9 (2017) 60, https://doi.org/10.1186/s13073-017-0450-0.
[15] H. Yin, R.L. Kanasty, A.A. Eltoukhy, A.J. Vegas, J.R. Dorkin, D.G. Anderson, Non-viral vectors for gene-based therapy, Nat. Rev. Genet. 15 (2014) 541–555, https://doi.org/10.1038/nrg3763.
[16] C. Lässer, S.C. Jang, J. Lötvall, Subpopulations of extracellular vesicles and their therapeutic potential, Mol. Asp. Med. 60 (2018) 1–14, https://doi.org/10.1016/j.mam.2018.02.002.
[17] H.-H. Wu, Y. Zhou, Y. Tabata, J.-Q. Gao, Mesenchymal stem cell-based drug delivery strategy: from cells to biomimetic, J. Control. Release 294 (2019) 102–113, https://doi.org/10.1016/j.jconrel.2018.12.019.
[18] N.E. Toledano Furman, Y. Lupu-Haber, T. Bronshtein, L. Kaneti, N. Letko, E. Weinstein, L. Baruch, M. Machluf, Reconstructed stem cell nanoghosts: a natural tumor targeting platform, Nano Lett. 13 (2013) 3248–3255, https://doi.org/10.1021/nl401376w.
[19] J. Oieni, L. Levy, N. Letko Khait, L. Yosef, B. Schoen, M. Fliman, H. Shalom-Luxenburg, N. Malkah Dayan, D. D'Atri, N. Cohen Anavy, M. Machluf, Nano-ghosts: biomimetic membranal vesicles, technology and characterization, Methods 177 (2019) 126–134. https://linkinghub.elsevier.com/retrieve/pii/S1046202319302701 (accessed December 22, 2019).
[20] Y. Lupu-Haber, T. Bronshtein, H. Shalom-Luxenburg, D. D'Atri, J. Oieni, L. Kaneti, A. Shagan, S. Hamias, L. Amram, G. Kaneti, N. Cohen Anavy, M. Machluf, Pretreating mesenchymal stem cells with cancer conditioned-media or proinflammatory cytokines changes the tumor and immune targeting by nanoghosts derived from these cells, Adv. Healthc. Mater. 8 (2019) 1801589, https://doi.org/10.1002/adhm.201801589.
[21] L. Kaneti, T. Bronshtein, N. Malkah Dayan, I. Kovregina, N. Letko Khait, Y. Lupu-Haber, M. Fliman, B.W. Schoen, G. Kaneti, M. MacHluf, Nanoghosts as a novel natural nonviral gene delivery platform safely targeting multiple cancers, Nano Lett. 16 (2016) 1574–1582, https://doi.org/10.1021/acs.nanolett.5b04237.
[22] N. Letko Khait, N. Malkah, G. Kaneti, L. Fried, N. Cohen Anavy, T. Bronshtein, M. Machluf, Radiolabeling of cell membrane-based nano-vesicles with 14C-linoleic acid for robust and sensitive quantification of their biodistribution, J. Control. Release 293 (2019) 215–223, https://doi.org/10.1016/j.jconrel.2018.12.005.
[23] M. Timaner, N. Letko-Khait, R. Kotsofruk, M. Benguigui, O. Beyar-Katz, C. Rachman-Tzemah, Z. Raviv, T. Bronshtein, M. Machluf, Y. Shaked, Therapy-educated mesenchymal stem cells enrich for tumor-initiating cells, Cancer Res. 78 (2018) 1253–1265, https://doi.org/10.1158/0008-5472.CAN-17-1547.
[24] A. Lolli, E. Lambertini, L. Penolazzi, M. Angelozzi, C. Morganti, T. Franceschetti, S. Pelucchi, R. Gambari, R. Piva, Pro-Chondrogenic effect of miR-221 and slug depletion in human MSCs, Stem Cell Rev. Rep. 10 (2014) 841–855, https://doi.org/10.1007/s12015-014-9532-1.
[25] A. Lolli, R. Narcisi, E. Lambertini, L. Penolazzi, M. Angelozzi, N. Kops, S. Gasparini, G.J.V.M. van Osch, R. Piva, Silencing of antichondrogenic MicroRNA-221 in human mesenchymal stem cells promotes cartilage repair in vivo, Stem Cells (2016), https://doi.org/10.1002/stem.2350.
[26] T. Bronshtein, N. Toledano, D. Danino, S. Pollack, M. Machluf, Cell derived liposomes expressing CCR5 as a new targeted drug-delivery system for HIV infected cells, J. Control. Release 151 (2011) 139–148, https://doi.org/10.1016/j.jconrel.2011.02.023.
[27] A. Lolli, K. Sivasubramaniyan, M.L. Vainieri, J. Oieni, N. Kops, A. Yayon, G.J.V.M. van Osch, Hydrogel-based delivery of antimiR-221 enhances cartilage regeneration by endogenous cells, J. Control. Release 309 (2019) 220–230, https://doi.org/10.1016/j.jconrel.2019.07.040.
[28] Y. Wang, L. Miao, A. Satterlee, L. Huang, Delivery of oligonucleotides with lipid nanoparticles, Adv. Drug Deliv. Rev. 87 (2015) 68–80, https://doi.org/10.1016/j.addr.2015.02.007.
[29] S.L. Loke, C.A. Stein, X.H. Zhang, K. Mori, M. Nakanishi, C. Subasinghe, J.S. Cohen, L.M. Neckers, Characterization of oligonucleotide transport into living cells, Proc. Natl. Acad. Sci. U. S. A. 86 (1989) 3474–3478, https://doi.org/10.1073/pnas.86.10.3474.
[30] S.M. Hoy, Patisiran: first global approval, Drugs. 78 (2018) 1625–1631, https://doi.org/10.1007/s40265-018-0983-6.
[31] L. Alvarez-Erviti, Y. Seow, H. Yin, C. Betts, S. Lakhal, M.J.A.A. Wood, Delivery of siRNA to the mouse brain by systemic injection of targeted exosomes, Nat. Biotechnol. 29 (2011) 341–345, https://doi.org/10.1038/nbt.1807.
[32] L. Wasungu, D. Hoekstra, Cationic lipids, lipoplexes and intracellular delivery of genes, J. Control. Release 116 (2006) 255–264, https://doi.org/10.1016/j.jconrel.2006.06.024.
[33] L.Y.T. Chou, K. Ming, W.C.W. Chan, Strategies for the intracellular delivery of nanoparticles, Chem. Soc. Rev. 40 (2011) 233–245, https://doi.org/10.1039/C0CS00003E.
[34] A. Parodi, N. Quattrocchi, A.L. van de Ven, C. Chiappini, M. Evangelopoulos, J. O. Martinez, B.S. Brown, S.Z. Khaled, I.K. Yazdi, M.V. Enzo, L. Isenhart, M. Ferrari, E. Tasciotti, Synthetic nanoparticles functionalized with biomimetic leukocyte membranes possess cell-like functions, Nat. Nanotechnol. 8 (2013) 61–68, https://doi.org/10.1038/nnano.2012.212.
[35] J.-W. Yoo, D.J. Irvine, D.E. Discher, S. Mitragotri, Bio-inspired, bioengineered and biomimetic drug delivery carriers, Nat. Rev. Drug Discov. 10 (2011) 521–535, https://doi.org/10.1038/nrd3499.
[36] G. Kim, M. Kim, Y. Lee, J.W. Byun, D.W. Hwang, M. Lee, Systemic delivery of microRNA-21 antisense oligonucleotides to the brain using T7-peptide decorated exosomes, J. Control. Release 317 (2020) 273–281, https://doi.org/10.1016/j.jconrel.2019.11.009.
[37] S.A.A. Kooijmans, S. Stremersch, K. Braeckmans, S.C. De Smedt, A. Hendrix, M.J. A. Wood, R.M. Schiffelers, K. Raemdonck, P. Vader, Electroporation-induced siRNA precipitation obscures the efficiency of siRNA loading into extracellular vesicles, J. Control. Release 172 (2013) 229–238, https://doi.org/10.1016/j.jconrel.2013.08.014.
[38] B. Heurtault, Physico-chemical stability of colloidal lipid particles, Biomaterials. 24 (2003) 4283–4300, https://doi.org/10.1016/S0142-9612(03)00331-4.

[39] D. Shi, X. Xu, Y. Ye, K. Song, Y. Cheng, J. Di, Q. Hu, J. Li, H. Ju, Q. Jiang, Z. Gu, Photo-cross-linked scaffold with Kartogenin-encapsulated nanoparticles for cartilage regeneration, ACS Nano 10 (2016) 1292–1299, https://doi.org/10.1021/acsnano.5b06663.
[40] M. Fathi-Achachelouei, D. Keskin, E. Bat, N.E. Vrana, A. Tezcaner, Dual growth factor delivery using PLGA nanoparticles in silk fibroin/PEGDMA hydrogels for articular cartilage tissue engineering, J. Biomed. Mater. Res. B Appl. Biomater (2019), https://doi.org/10.1002/jbm.b.34544 jbm.b.34544.
[41] A.L.Z. Lee, Z.X. Voo, W. Chin, R.J. Ono, C. Yang, S. Gao, J.L. Hedrick, Y.Y. Yang, Injectable coacervate hydrogel for delivery of anticancer drug-loaded nanoparticles in vivo, ACS Appl. Mater. Interfaces 10 (2018) 13274–13282, https://doi.org/10.1021/acsami.7b14319.
[42] S. Salatin, J. Barar, M. Barzegar-Jalali, K. Adibkia, M.A. Milani, M. Jelvehgari, Hydrogel nanoparticles and nanocomposites for nasal drug/vaccine delivery, Arch. Pharm. Res. 39 (2016) 1181–1192, https://doi.org/10.1007/s12272-016-0782-0.
[43] Z. Li, K.M. Kaplan, A. Wertzel, M. Peroglio, B. Amit, M. Alini, S. Grad, A. Yayon, Biomimetic fibrin–hyaluronan hydrogels for nucleus pulposus regeneration, Regen. Med. 9 (2014) 309–326, https://doi.org/10.2217/rme.14.5.
[44] L. Kandel, G. Agar, O. Elkayam, A. Sharipov, O. Slevin, G. Rivkin, M. Dahan, V. Aloush, A.B. Pyeser, Y. Brin, Y. Beer, A. Yayon, A novel approach for knee osteoarthritis using high molecular weight hyaluronic acid conjugated to plasma fibrinogen – interim findings of a double-blind clinical study, Heliyon. 6 (2020), e04475, https://doi.org/10.1016/j.heliyon.2020.e04475.
[45] M.L. Vainieri, A. Lolli, N. Kops, D. D'Atri, D. Eglin, A. Yayon, M. Alini, S. Grad, K. Sivasubramaniyan, G.J.V.M. van Osch, Evaluation of biomimetic hyaluronic-based hydrogels with enhanced endogenous cell recruitment and cartilage matrix formation, Acta Biomater. 101 (2020) 293–303, https://doi.org/10.1016/j.actbio.2019.11.015.
[46] R.S. Riley, C.H. June, R. Langer, M.J. Mitchell, Delivery technologies for cancer immunotherapy, Nat. Rev. Drug Discov. 18 (2019) 175–196, https://doi.org/10.1038/s41573-018-0006-z.
[47] J. Reinholz, K. Landfester, V. Mailänder, The challenges of oral drug delivery via nanocarriers, Drug Deliv. 25 (2018) 1694–1705, https://doi.org/10.1080/10717544.2018.1501119.
[48] C.H. Evans, V.B. Kraus, L.A. Setton, Progress in intra-articular therapy, Nat. Rev. Rheumatol. 10 (2014) 11–22, https://doi.org/10.1038/nrrheum.2013.159.
[49] F. Colella, J.P. Garcia, M. Sorbona, A. Lolli, B. Antunes, D. D'Atri, F.P.Y. Barré, J. Oieni, M.L. Vainieri, L. Zerrillo, S. Capar, S. Häckel, Y. Cai, L.B. Creemers, Drug delivery in intervertebral disc degeneration and osteoarthritis: selecting the optimal platform for the delivery of disease-modifying agents, J. Control. Release 328 (2020) 985–999.